Improved Selectivity and Sensitivity of Gas Sensing Using a 3D Reduced Graphene Oxide Hydrogel with an Integrated Microheater

Wu, Jin; Tao, Kai; Miao, Jianmin; Norford, Leslie K.

2015

Wu, J., Tao, K., Miao, J., & Norford, L. K. (2015). Improved Selectivity and Sensitivity of Gas Sensing Using a 3D Reduced Graphene Oxide Hydrogel with an Integrated Microheater. ACS Applied Materials & Interfaces, 7(49), 27502-27510.

https://hdl.handle.net/10356/81603

https://doi.org/10.1021/acsami.5b09695

ACS APPLIED MATERIALS & INTERFACES

Research Article

www.acsami.org

Improved Selectivity and Sensitivity of Gas Sensing Using a 3D Reduced Graphene Oxide Hydrogel with an Integrated Microheater

Jin Wu,[†] Kai Tao,[†] Jianmin Miao,*[,†] and Leslie K. Norford[‡,§]

[†]School of Mechanical and Aerospace Engineering, Nanyang Technological University, Singapore 639798, Singapore

[‡]Center for Environmental Sensing and Modeling (CENSAM), Singapore-MIT Alliance for Research and Technology (SMART) Centre, Singapore 117543, Singapore

[§]Department of Architecture, Massachusetts Institute of Technology, Cambridge, Massachusetts 02139, United States

Supporting Information

ABSTRACT: Low-cost, one-step, and hydrothermal synthesized 3D reduced graphene oxide hydrogel (RGOH) is exploited to fabricate a high performance NO_2 and NH_3 sensor with an integrated microheater. The sensor can experimentally detect NO_2 and NH_3 at low concentrations of 200 ppb and 20 ppm, respectively, at room temperature. In addition to accelerating the signal recovery rate by elevating the local silicon substrate temperature, the microheater is exploited for the first time to improve the selectivity of NO_2 sensing. Specifically, the sensor response from NH_3 can be effectively suppressed by a locally increased temperature, while the sensitivity of detecting NO_2 is not significantly affected. This leads to good discrimination between NO_2 and NH_3. This strategy paves a new avenue to improve the selectivity of gas sensing by using the microheater to raise substrate temperature.

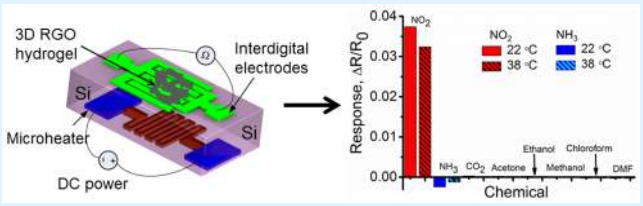

KEYWORDS: *reduced graphene oxide hydrogel, gas sensor, three-dimensional structures, selectivity, NO_2, microheater*

INTRODUCTION

Continued development of industry and agriculture brings increased production and emission of toxic, combustible, and flammable gases.[1−7] Among them, NO_x, O_3, SO_2, CO, and ammonia (NH_3) are the most common and harmful air pollutants, which endanger human health in the long term.[8] Development of highly sensitive, highly selective, and cost-effective gas sensors that enable monitoring of environmental pollutants and detection of trace chemicals is important for both industrial and civilian purposes.[2,4] Such materials as inorganic semiconductors, conductive polymers, optical fibers, carbon nanotubes, and two-dimensional materials have been exploited as effective gas sensing elements.[3,9−12] Among them, graphene (Gr) has recently attracted intense attention in gas sensing because of its atom-thick two-dimensional conjugated structures, large surface areas, low electrical noise, high conductivity, and outstanding electronic properties.[2,3,13] Reduced graphene oxide (RGO) possesses a high surface-to-volume ratio, which provides sufficient surface areas and defects for gas adsorption, reaction, and catalytic activities.[2,14] RGO conveniently interacts with gas adsorbates from weak van der Waals forces to strong covalent bonding.[3] Both of them can alter the local carrier density of RGO, changing the electrical resistance. RGO has inherently low electrical noise due to its two-dimensional, atomic-scale, and high-quality hexagonal lattice.[3] Hence, very little charge transfer between RGO and gas can induce a noticeable change of its resistance.[4] Furthermore, RGO can be modified with other functional groups or hybridized with other sensing materials to improve its sensitivity and selectivity.[2,3,15] Finally, a variety of strategies can be employed to produce high-quality Gr, chemically modified RGO, and derived hybridization in a low-cost and large-scale manner.[2] Since Gr/RGO shows unique and attractive merits for gas sensing, it holds significant potential for future practical applications.[1,14]

Until now, pristine Gr, modified RGO, and RGO composite have been deployed to construct high-performance gas sensors.[3,16−19] However, most Gr-based gas sensors focus on the utilization of 2D Gr nanosheets, and little attention has been paid to 3D Gr. 3D Gr/RGO has recently exhibited many advantages, such as increased surface areas and reactive sites, which make it an attractive alternative for gas sensing, supercapacitors, and other electrochemical applications.[2,20−26] For 3D Gr gas sensors, the enlarged interaction surface areas enhance the sensing performance, including higher sensitivity, faster response, and even a lower limit of detection (LOD) for particular gases.[2,13,27] Although several examples of 3D Gr/RGO based gas sensors have been reported to display good performance, these strategies suffer from either a complex fabrication process or high cost. For instance, a macroscopic foam-like 3D Gr network fabricated by chemical vapor deposition (CVD) has been used for highly sensitive gas

Received: October 12, 2015
Accepted: November 24, 2015
Published: November 24, 2015

DOI: 10.1021/acsami.5b09695
ACS Appl. Mater. Interfaces 2015, 7, 27502−27510

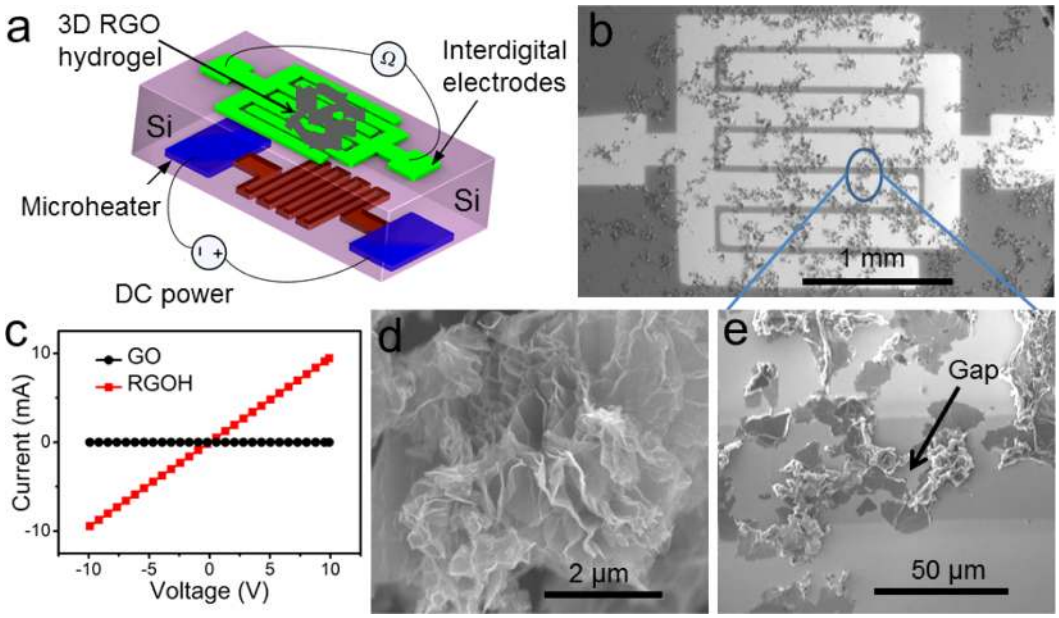

Figure 1. (a) Schematic illustrating a 3D RGOH-based gas sensor with an integrated microheater. The interdigital electrodes that were bridged by RGOH were fabricated on the top side of the Si/SiO_2 wafer, while the microheater was fabricated on the bottom side. (b) Low-magnification SEM image of the RGOH bridged interdigital electrodes. (c) Room temperature I–V curves of GO and RGOH that were deposited on interdigital electrodes and measured by a two-probe method. The RGOH exhibits an Ohmic conductive characteristic, while GO is nearly insulating. (d) High-magnification SEM image showing the interior 3D porous nanostructures of RGOH. (e) SEM image showing one of the RGOH-bridged gaps on the interdigital electrodes in (b).

detection.[13,24] However, the CVD synthesis methodology intrinsically demands expensive equipment, high temperature, and a vacuum environment, which increases fabrication cost. Additionally, 2D RGO nanosheets assembled on micropatterned 3D SU8 micropillar arrays have been employed to improve the sensing performance compared to a corresponding 2D planar RGO-based sensor.[2] However, costly lithography is needed to fabricate the 3D SU8 pillars.[2,28] Furthermore, atomic layer deposition of a layer of transitional Al_2O_3 on the pillars and chemical modification of the Al_2O_3 surface are required to enable the adsorption of (Graphene Oxide) GO nanosheets on SU8 pillars,[2] which complicates the device fabrication. Both of the above-mentioned two-step methodologies for preparation of gas sensors require external templates such as nickel foam and SU-8 pillars to construct 3D Gr/RGO structures.

In this work, we demonstrate that the 3D reduced graphene oxide hydrogel (RGOH) synthesized by a one-step, hydrothermal, and self-assembly method can be used for high performance gas sensing (Figure 1a). Since the sensing materials themselves are assembled as 3D porous micro-/nanostructures, the complicated and expensive fabrication of 3D templates is bypassed. We find that the 3D RGOH sensor can detect NO_2 in air with parts-per-billion concentrations. This method of fabricating 3D RGO-based gas sensor is facile, cost-effective, and simple compared to previously reported strategies. Furthermore, a miniaturized microheater is integrated in the gas sensor to investigate temperature-dependent gas sensing performance. For the first time, we find that an elevated temperature can significantly reduce the sensitivity of detecting NH_3, without significantly deteriorating the sensitivity of detecting the target gas, NO_2. Therefore, the locally raised temperature allows for the improvement of selectivity of NO_2 detection. Furthermore, it is found that the microheater can accelerate the signal recovery process, which is desirable for practical gas sensing applications.

METHODS

Synthesis of GO. GO was prepared from graphite powder via Hummer's method.[20,29] Briefly, graphite (3.0 g) was added to concentrated sulfuric acid (69 mL) while stirring, followed by the addition of sodium nitrate (1.5 g). The mixture was cooled to 0 °C. Subsequently, potassium permanganate (9.0 g) was added slowly to keep the reaction temperature below 20 °C. After the reaction system was slowly transferred to a 35 °C water bath for 30 min, 138 mL water was added slowly, and the solution was stirred for another 15 min. Additional water (420 mL) and 30% H_2O_2 (3 mL) were added, making the color of the solution change from brown to yellow. After air cooling, the mixture was filtered and washed with 1:10 HCl aqueous solution (250 mL) to remove metal ions. The removal of acid can be made by repeated washing with water and centrifugation. The obtained solid was dispersed in water by ultrasonication for 40 min. The resulting GO aqueous dispersion was subjected to centrifugation at 3800 rpm for 35 min to remove aggregates. Finally, the remaining salt impurities were removed by dialysis for the following application.

Preparation of Self-Assembled RGOH. RGOH was synthesized according to a previously reported method.[20] The typical RGOH can be hydrothermally synthesized simply by putting 2 mg/mL of homogeneous GO aqueous dispersion in a sealed Teflon-lined autoclave and heating the system at 180 °C for 10 h. Then the autoclave was naturally cooled to room temperature and the as-prepared RGOH was taken out with a tweezer. The surface adsorbed water of RGOH was removed by a filter paper. Finally, a certain amount of RGOH solid was redispersed in water by ultrasonication to form a homogeneous 1 mg/mL aqueous dispersion of RGOH.

Fabrication of 3D RGOH Sensors. The interdigital electrodes were fabricated by thermal evaporation of 5 nm Cr/60 nm Au on an oxidized silicon wafer (300 μm thick, with a 300 nm thick SiO_2 layer on both sides) using a shadow mask. The gap between adjacent gold strips was 40 μm. Before drop casting the RGOH aqueous dispersion, the silicon wafers were treated with oxygen plasma at 20 mW for 3 min to render them hydrophilic. After drop casting the RGOH aqueous dispersion on the Au interdigital electrodes, the dispersion spread on the substrate due to adequate wetting of the substrate. After water drying, the RGOH bridged the gaps on the interdigital electrodes,

DOI: 10.1021/acsami.5b09695
ACS Appl. Mater. Interfaces 2015, 7, 27502–27510

which made them conductive and the sensor capable of detecting certain gases. FE-SEM 7600 was deployed to characterize the morphology of the RGOH, RGOH bridged interdigital electrodes and the microheater.

Fabrication and Characterization of the Microheater. Microfabrication and micromachining technologies were exploited to fabricate microheaters on the backside of the silicon wafer,[30] on the front side of which the RGOH bridged interdigital electrodes were fabricated. First, a 5 μm thick AZ 9260 photoresist layer was spin coated on the Si wafer, followed by photolithography, sputtering of 10 nm Cr/300 nm Pt and lifting off the photoresist to pattern platinum (Pt) heating lines (300 nm thick) onto the substrate. The gold (Au) contacting pads (300 nm thick) were patterned in the same way by another photolithography, sputtering and lift-off process. The microheater has serpentine Pt lines with width of 25 μm and the contact pad size of 1 × 1 mm^2. In order to generate sufficient heat using low voltage and low power consumption, four microheaters were electrically connected in parallel to an external direct current (DC) power supply to reduce the resistance of the system. When a DC voltage was applied on the electrodes of the microheater, the Joule effect of the integrated microheater quickly heated the device to the desired temperature, which was measured in situ by an infrared camera (TYPE F30W, NEC Avio Infrared Technologies Co., Ltd.).

Gas Sensing Measurement. Sensing measurements were performed in a gas chamber using two terminal devices. Dry synthetic air was exploited as a carrier gas to dilute the test gas and purge the devices after stopping the test gas feeding. The flow rate of the carrier gas was kept at a constant (500 sccm). For the NO_2 gas source with an initial NO_2 concentration of 10 ppm in pure nitrogen, the NO_2 gas concentration could be tuned from 10 ppm to 200 ppb by diluting the gas source based on our experimental setup. For the NH_3 gas source with an initial concentration of 1000 ppm, the test gas concentration could be adjusted from 1000 to 20 ppm by diluting the gas source. The applied voltage between the two electrodes was 0.1 V. Volatile organic compounds such as methanol and toluene were delivered using a saturated vapor stream at room temperature. For all responses and recovery percent presented in the figures, five different samples were measured to obtain average values. Error bars shown in the figures were obtained from the standard deviation of the responses or recovery percent of the five samples.

RESULTS AND DISCUSSION

Characterization of 3D RGOH. Figure 1b and d–e exhibits scanning electron micrograph (SEM) images of RGOH as deposited on the interdigital electrodes. We can clearly see the three-dimensional, porous and interconnected micro/nanostructures of the 3D agglomerates of RGO. The pore sizes of the 3D network range from several hundred nanometers to tens of micrometers. The walls of the pores are composed of thin RGO sheets, assembled together at the physical cross-linking sites to form 3D agglomerated nanostructures.[20] The resistance decreased from ~10^{11} Ω of GO to 1000 Ω of RGOH, which confirmed the successful conversion of insulating GO into conductive RGOH (Figure 1c). The good conductivity of RGOH makes it suitable for gas sensing application.

X-ray diffraction (XRD) patterns demonstrate the effective deoxygenation of GO, leading to the formation of a microporous network of RGOH upon hydrothermal reduction (Figure 2).[31] The XRD peak of freeze-dried RGOH is broad, which suggests that the Gr sheets are ordered poorly along their stacking direction and that the 3D RGOH mesh consists of layers of Gr nanosheets.[20] From the XRD patterns, the interlayer spacing of the freeze-dried RGOH is calculated by Bragg's law to be 3.7 Å, which is much smaller than that of the GO precursor (6.95 Å) and slightly larger than that of graphite (3.35 Å).[31] It indicates that the Gr sheets agglomerate into a

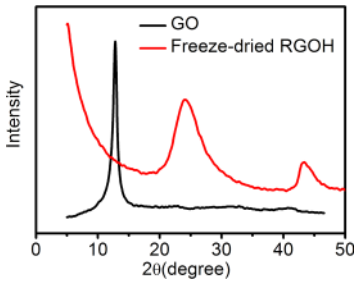

Figure 2. XRD patterns of GO (black) and freeze-dried RGOH (red).

3D RGOH mesh, which is consistent with the morphology of the RGOH characterized by SEM (Figure 1d). The recovery of π-conjugated system of RGOH also leads to good conductivity, which agrees well with the measured I–V curves in Figure 1c.

Characterization of Microheater. Although an external heater can be deployed to rapidly achieve complete desorption of gas, it makes the device bulky, complicated and not portable. Because of the low thermal conductivity of the SiO_2 layer (~1 W m^{-1} K^{-1}) on the Si/SiO_2 substrate, a microheater imbedded on the substrate can introduce a local heating effect with low power consumption and miniaturized device size, which favors portability.[30] When a DC voltage U is applied to the microheater, the Pt resistor heats the substrate due to the Joule effect with the power of $P = U^2/R$, in which R is the resistance of microheater. The resistance can be determined by $R = \rho l/(tw)$, where ρ, l, t, and w are electrical resistivity, length, thickness and width of the resistor, respectively. The 25 μm wide serpentine Pt lines shown in Figure 3a play the key role in heating, while other metal lines serve as bonding pads. As such, electrical wires on the substrate are much wider (e.g., the Au contact pads have the size of 1 × 1 mm^2). In this case, the resistance of the microheater is dominated by the Pt lines, which generate the majority of heat and temperature much higher than other parts of the substrate.

Generally, the temperature-resistance relationship of a microheater can be expressed by the following eq 1:

$$R = R_0[1 + \alpha(T - T_0)] = (R_0 - \alpha R_0 T_0) + \alpha R_0 T \quad (1)$$

where α is the temperature coefficient of resistance (TCR) of the resistor, and R_0 is the resistance at the reference temperature T_0 = 20 °C.[30] Figure 3b shows that the current and the average temperature of the microheater rise monotonously with the increased voltage. The slope of the current–voltage (I–V) curve gradually reduces because of the incremental change of the resistance of the microheater at elevated temperatures. The experimental obtained relationship between the temperature and the resistance of the microheater (dash-dot black line in Figure 3c) can be linearly fitted as R = 0.32664T + 76.417, as shown as the red line in Figure 3c. Comparing with eq 1, we obtain $R_0 - \alpha R_0 T_0$ = 76.417 and αR_0 = 0.32664. Thus, the corresponding TCR can be calculated as $\alpha \approx$ 0.00394 °C^{-1}, which is consistent with that of pure Pt ($\alpha \approx$ 0.0039 °C^{-1}).[30] Hence, the temperature of the microheater can be monitored by measuring the resistance according to eq 1 and local temperatures of the substrate can be adjusted conveniently by programming the applied voltage (Figure 3b–c). The infrared camera captured an optical image of the substrate on the RGOH side, showing that the substrate was heated to 38 °C with the applied voltage of 5 V (Figure 3d). An increase of voltage caused the temperature of substrate to rise (Figure S1).

DOI: 10.1021/acsami.5b09695
ACS Appl. Mater. Interfaces 2015, 7, 27502–27510

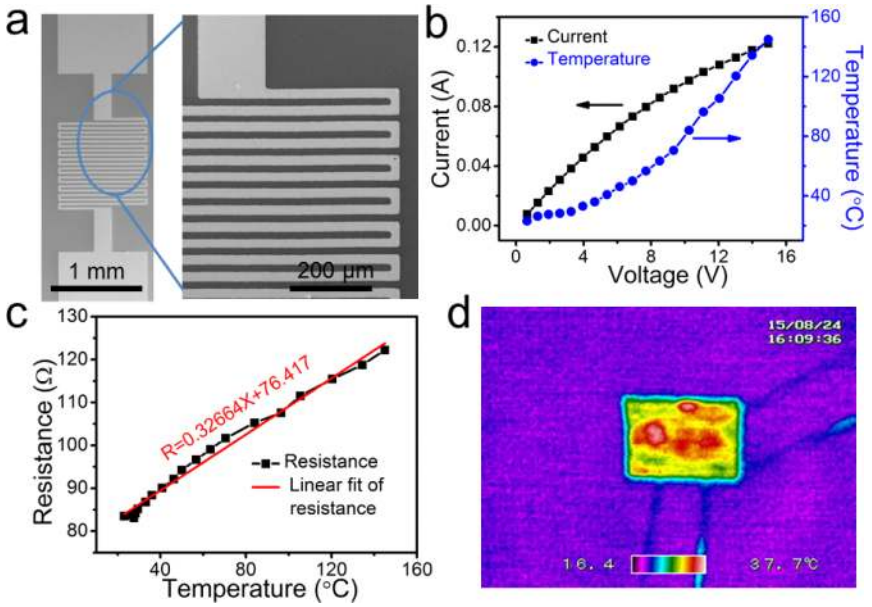

Figure 3. Characterization of the microheater. (a) SEM images of a single microheater (left) and magnified Pt lines on the microheater (right). (b) The current and the temperature of the microheater at different voltages. (c) The calculated (dash-dot black line) and linearly fitted (straight red line) resistance versus temperature curves of the microheater. (d) The infrared camera captured optical image of the gas sensor when the DC voltage of 5 V was applied to the microheater.

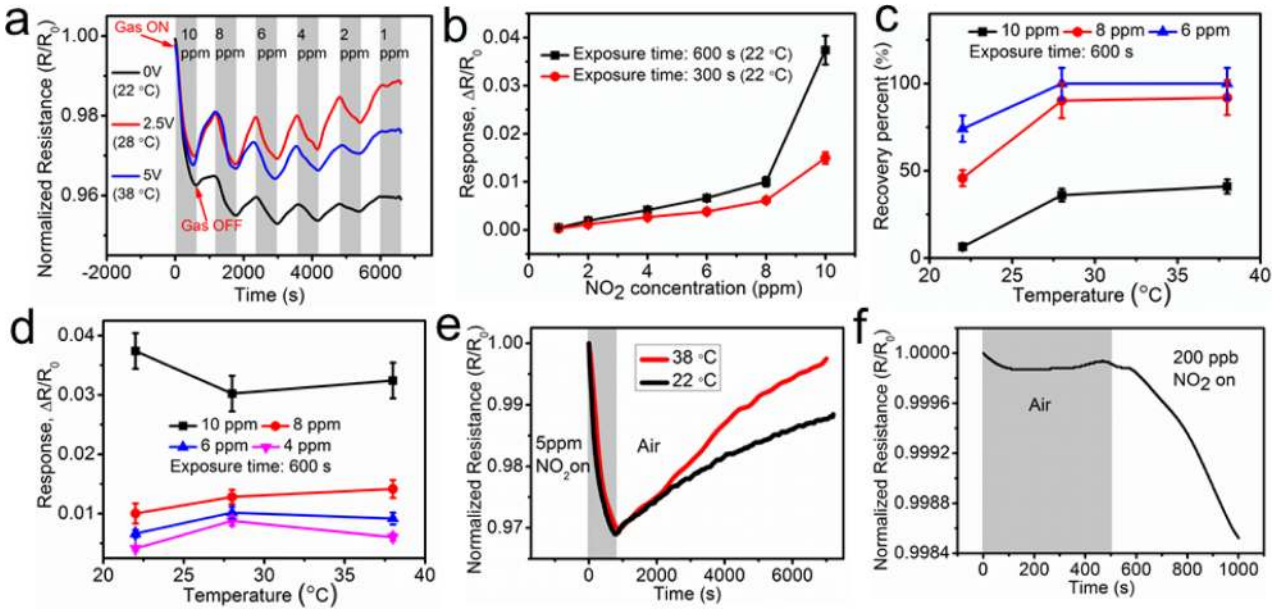

Figure 4. NO_2 detection. (a) Responsiveness of the RGOH sensor to NO_2 of various concentrations at 22, 28, and 38 °C, respectively. (b) Response of the RGOH sensor to different NO_2 concentrations at the exposure times of 600 and 300 s, respectively. (c and d) Signal recovery percentage and quantitative response of the RGOH sensor respectively at different temperatures with both the exposure time and air purge time of 600 s. (e) Investigation of the signal recovery process of 5 ppm of NO_2 sensing by prolonging the air purge time to 6200 s at 22 and 38 °C, respectively. (f) Response of the RGOH sensor to 200 ppb NO_2. Gray and white vertical strips correspond to periods of time when the flow of NO_2 is turned on and off, respectively.

NO_2 Sensing. The normalized resistance is plotted as R/R_0, where R_0 and R are the resistance measured before and after gas exposure, respectively. And the response is defined as $(R_0 - R)/R_0 = \Delta R/R_0$. The signal recovery percent is defined as the ratio of the change of resistance in an air purge process to that in the target gas exposure process. The RGOH sensor exhibited an obvious resistance change when it was exposed to NO_2 gas with the concentration decreasing from 10 ppm to 200 ppb (Figure 4). The resistance of the RGOH sensor reduced noticeably when NO_2 was introduced. Furthermore, the response decreased monotonically from 3.74% to 0.19% when the concentration of NO_2 gas was reduced from 10 to 2 ppm at the exposure time of 600 s (Figure 4a–b). We found that the response decreased from 3.74% to 1.5% with shortened gas exposure time from 600 to 300 s for 10 ppm of NO_2 (Figure 4b), demonstrating that the gas adsorption process needed sufficient time to reach saturation. Possibly the residual oxygen defects such as epoxides and carboxylic acids in RGOH

DOI: 10.1021/acsami.5b09695
ACS Appl. Mater. Interfaces 2015, 7, 27502–27510

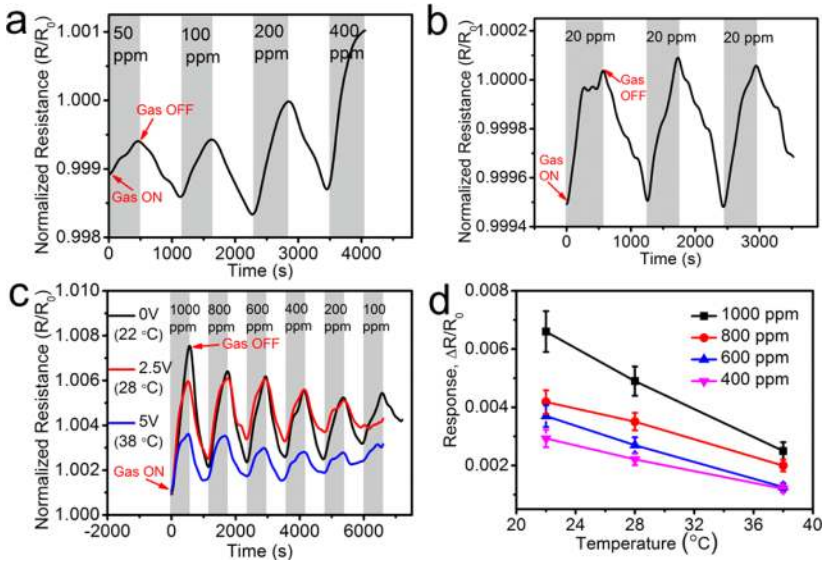

Figure 5. NH_3 sensing. (a) Response of the RGOH sensor to NH_3 with the concentrations increasing from 50 to 400 ppm at 22 °C. (b) Detection of 20 ppm of NH_3 with good repeatability and signal reversibility at 22 °C. (c) Response of the RGOH sensor to NH_3 at different temperatures. (d) Temperature-dependent response of the RGOH sensor to NH_3 of different concentrations. The NH_3 exposure time and the air purge time are 600 s in all parts of the figure.

result in higher binding energies and lead to the longer response times.[1] Notice that the response is a little adversely affected with rise in temperature, but the influence is not strong at low temperature. For example, the responses of the sensor to 10 ppm of NO_2 are 3.74%, 3.02%, and 3.24% at the temperatures 22, 28, and 38 °C respectively (Figure 4d). This reveals that the sensor shows the best response to 10 ppm of NO_2 at 22 °C. However, when the temperature is further elevated to 55 °C or higher by the microheater, the response is seriously deteriorated (Figure S2), demonstrating that an appropriate temperature is essential to maintain the sensitivity of NO_2 detection. Importantly, the elevated temperature led to significantly increased signal recovery percentage within the same purge time, an indication of the accelerated signal recovery rate and therefore better reversibility of the device (Figure 4c). For instance, the recovery percent increased from 45% at 22 °C to 92% at 38 °C within 600 s for 8 ppm of NO_2 with the help of the microheater to accelerate the gas desorption. Possibly the locally elevated temperature can help to expel chemisorbed molecules from the RGOH's surface by exciting the molecules to vibrate so that they become a pulsive state.[13,32] There is a competition between adsorption energy and thermal energy for the gas release. As the temperature rises, the adsorption energy decreases,[33] while the thermal energy increases. Thus, the response is adversely affected with raised temperature. However, the recovery is positively affected by elevated temperature. This is because the heating facilitates the recovery by lowering the energy barrier of the desorption of gas molecules, which bypasses the demand of ultraviolet light illumination.[34] To further investigate the signal recovery process, we purposely prolonged the air purge period after exposure to 5 ppm of NO_2. It was found that the signal only reached the recovery percentage of 61.2% after air purge for 6200 s (Figure 4e). However, with the temperature elevated to 38 °C, the signal recovery percentage reached 91.3%. This demonstrates that the microheater gives fast signal recovery, which is significant for the practical application of gas sensors.[1,2,13] To investigate the device-to-device reproducibility of the sensors, we employed five different samples to obtain a statistical response. It is found that the response variation is around 10.1%, indicative of good repeatability of the gas sensor (error bars in Figure 4b–d).

Since the response in the first exposure to 10 ppm of NO_2 was much larger than that in the subsequent exposure to 8 ppm of NO_2, the curves of response versus concentration were not linear when the concentration of NO_2 reduced from 10 to 1 ppm (Figure 4a–b). This can be attributed to incomplete recovery in the first exposure to NO_2 with high concentration, which results from slow out-diffusion of gas molecules in the multilayer stacking nanostructures of the 3D RGOH network. The gas molecules diffuse between the stacks of Gr sheets in 3D RGOH after exposure to the gas, leading to increased response. However, the diffuse of the gas molecules out of the stack gaps is slow in the air purge process. Possibly, the introduction of a high concentration of NO_2 in the first exposure makes the gas adsorb not only on the edges, but also on the basal plane of a Gr sheet. The gas adsorption and desorption on the surfaces and edges is faster. However, the gas molecules adsorbed on the basal plane cannot be easily expelled completely during the air purge process. Hence, the capability of adsorbing new NO_2 molecules was weakened during later exposure to 8 ppm of NO_2 process. However, the plot of the response versus NO_2 concentration exhibited an obviously linear region from 1 to 8 ppm (Figure 4b). In contrast to the nonlinear curves of response versus concentration when NO_2 was introduced from high to low concentration, the curve of response versus concentration was almost linear when NO_2 was introduced from low to high concentration (Figure S3). According to the International Union of Pure and Applied Chemistry (IUPAC), theoretical LOD can be obtained when the signal is three times more than the noise.[2,35] The theoretical LOD can be calculated from the slope of the linear region of the response curve and the root-mean-square (RMS) deviation at the baseline.[2,36] The theoretical LOD of 186 ± 8.1 ppb for NO_2 sensing was obtained by using this calculation method (Figure S4 and Tables S1–S2). Notice that the RGOH sensor

DOI: 10.1021/acsami.5b09695
ACS Appl. Mater. Interfaces 2015, 7, 27502–27510

can detect the NO_2 with the low concentration of 200 ppb experimentally (Figure 4f), which agrees well with the theoretically calculated result. The theoretically and experimentally achieved LODs by this 3D RGOH sensor are much lower than those of previously reported 3D Gr/RGO based NO_2 sensors.[2,13,27,37,38] Based on the Langmuir adsorption isotherm, the relationship between sensor response and gas concentration was derived,[33,34] which could be utilized to predict a LOD of 187 ppb and the saturated response of 4.8% for NO_2 sensing (Figure S5). The LOD calculated by the aforementioned two methods is consistent. However, the sensing performance of the 3D RGOH sensor is compromised by the small response compared to that of previously reported Gr or carbon nanotubes (CNT) based sensors.[1,2,33,34,39,40] Such a small response may arise from our homemade gas sensing characterization system, since the sensing chamber is not isolated very well from outside. Previously, it is reported that the recovery rate of Gr and CNT-based sensing device can be accelerated by heating or UV exposure.[36,41,42] However, the heat and UV light sources are relatively bulky. In this work, the microheater integrated in the gas sensor offers the advantages of miniaturized device size, reduced power consumption and improved thermal safety. In order to calibrate the sensor, the resistance of the RGOH device was measured as a function of temperature (Figure S6a). It was found that the RGOH displayed a semiconducting behavior with a negative coefficient of thermal resistivity of about 7.05 V/K. After applying voltage to the microheater, the resistance decreased quickly, stabilizing in less than 100 s (Figure S6b).

NH_3 Detection. In addition to NO_2, the RGOH sensor also displayed good response to NH_3 (Figure 5). The responsiveness rose with the increased concentration of NH_3 (Figure S7). Importantly, the RGOH sensor showed good repeatability and reversibility to NH_3 with the concentration of 20 ppm, which was the lowest NH_3 concentration allowed by our gas sensing system (Figure 5b). The capability to detect NO_2 < 3 ppm and NH_3 < 25 ppm is important for practical sensors.[2,43] Our sensors were accurately responsive to NO_2 at a concentration much lower than 3 ppm and NH_3 at a concentration below 25 ppm. In contrast with NO_2 detection, the sensitivity of NH_3 sensing decreased significantly with elevated temperature (Figure 5c–d). Taking the detection of 1000 ppm of NH_3 as an example, the response reduced from 0.67% to 0.25% when the temperature of the substrate was elevated from 22 to 38 °C. Possibly the elevated temperature facilitates the desorption of NH_3 molecules from RGOH and therefore weakens the sensor's capability of adsorbing NH_3 molecules. Notice that the introduction of NO_2 in the gas chamber led to decreased resistance of the RGOH sensor, while the exposure to NH_3 caused increased resistance. The opposite resistance change trends for NO_2 and NH_3 facilitate the differentiation between the two gases. The resistance change of RGOH is attributed to charge transfer between RGOH and adsorbed gas molecules.[1,2,13] The oxygen containing groups such as residual carboxylic and epoxide groups and water molecules existing in chemically produced RGOH generate some holes into the conduction band, which makes RGOH behave as a p-type semiconductor.[1,3,44] The Seebeck coefficient can also be employed to explore the type of carrier in measured materials.[44,45] For example, the Seebeck coefficient is negative for negatively charged carriers (such as electrons), and positive for positively charged carriers (such as holes).[45,46] In our work, we identified the type of carrier in RGOH by measuring the Seebeck coefficient of 3D RGOH for the first time (Figure S8). It was found that the measured Seebeck coefficient of RGOH displayed a positive value from 35 to 65 °C, indicating the p-type semiconducting characteristic of RGOH. In addition, the measured Seebeck coefficient of the 3D RGOH (300 μV/K at 35 °C) is much higher than that of previously reported monolayer or multiple layer Gr,[44] which may be attributed to the effect of disorder induced scattering and defects in multiple-layer Gr stacked 3D RGOH.[44,47] For example, it is reported that the Seebeck coefficient of multiple-layered Gr increases monotonically with added layer and reaches its maximum value at a hexalayer.[44] Due to the p-type doping of RGOH, the adsorption of p-type dopants, such as NO_2, enhances hole conduction and leads to a significant decrease in resistance, while the adsorption of n-type dopants, such as NH_3, decreases hole conduction and therefore causes the increase in resistance.[1,2]

Improved Selectivity via Microheater. The capability of the microheater to suppress the response of the RGOH sensor to NH_3 without significantly deteriorating the response to NO_2 at elevated temperature provides an effective discrimination between NO_2 and NH_3. For example, the response of the RGOH sensor to NH_3 at 38 °C was less than half of that at 22 °C, while the response to NO_2 only changed 13% from 22 to 38 °C (Figure 6). Here, we utilize the adsorption energy (E_{ad})

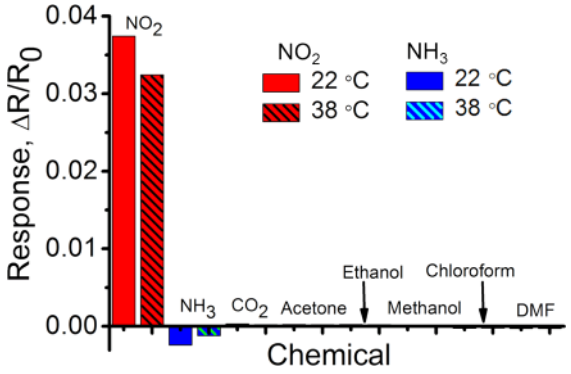

Figure 6. Response of the RGOH sensor to different gaseous chemicals, including 10 ppm of NO_2, 400 ppm of NH_3, 600 ppm of CO_2, and other organic chemical vapors at different temperatures. The solid and lined bars correspond to the responses at 22 and 38 °C, respectively. The positive and negative values of the response correspond to decreased and increased resistance upon exposure to these gases.

between Gr and different gas molecules to explain the enhanced selectivity at elevated temperature. According to a first-principles study in previous research, the defective Gr shows much higher adsorption energy with NO_2 (−3.04 eV) than that with NH_3 (−0.24 eV).[48] Hence, the defective Gr displays much stronger interaction with NO_2 molecules than that with NH_3 molecules. In the case of locally increased temperature by the microheater, the adhesion between the defective Gr and NH_3 molecules become less stable compared with that between the Gr and NO_2 molecules. Hence, the elevated temperature reduces the sensitivity of NH_3 detection significantly, but does not affect the sensitivity of NO_2 sensing greatly, leading to improved selectivity of NO_2 sensing. To the best of our knowledge, this is the first time that the locally elevated temperature is employed to enhance the selectivity of RGO based gas sensing. In previous research, although it was

DOI: 10.1021/acsami.5b09695
ACS Appl. Mater. Interfaces 2015, 7, 27502–27510

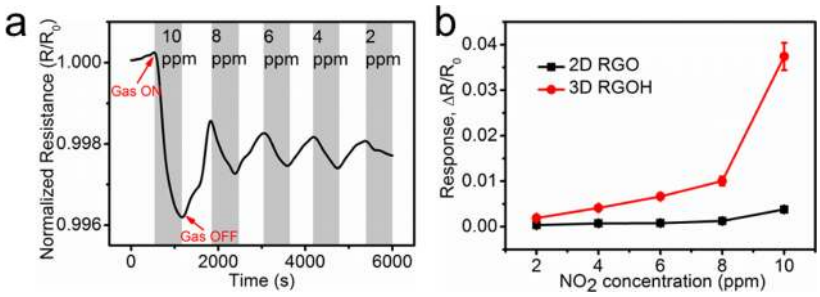

Figure 7. (a) Response of a 2D RGO nanosheet based sensor to NO_2 of different concentrations. (b) Comparison between the response of 3D RGOH and that of 2D RGO nanosheets to NO_2 of different concentrations.

reported that the elevated temperature could be used to speed up the recovery process at the expense of sensitivity,[1,2,13,49−51] the dependence of selectivity on temperature was never explored. It demonstrates that the microheater gives very fast temperature modulation and control to characterize the sensing materials and boost the gas sensing performance, including improved selectivity, recovery and data interpretation. This method may shed light on the improvement of the selectivity of various chemical sensing devices.[12,52] In contrast to NO_2 and NH_3, the RGOH sensor displays little response to other gases such as various gaseous organic chemicals (Figure 6), an indication of good selectivity. Possibly, in addition to adsorbing on the surface of RGOH, NO_2 and NH_3 molecules can also penetrate and diffuse between the stacks of 3D RGOH due to relatively high adsorption energy, making the resistance change greatly.[13,27,48] In contrast, molecules of alcohols such as ethanol and methanol only interact with the top few layers of the 3D RGOH stacks, resulting in smaller resistance change and reduced response.[53,54] To compare the NO_2 sensing performance of 3D RGOH with that of 2D RGO nanosheets, we deposited 2 mg/mL homogeneous GO aqueous dispersion on the interdigital electrodes by drop casting, followed by reduction of the GO to RGO by exposure to hydrazine vapor up to 24 h at 100 °C. It was found that the response of the 3D RGOH was 10 times higher than that of 2D RGO nanosheets with the same experimental conditions (Figure 7). Probably the improved gas sensing performance of the 3D RGOH results from its enlarged interaction surface areas and increased reactive sites.[2,13]

CONCLUSIONS

We have successfully fabricated a highly selective and sensitive gas sensor by exploiting a one-step hydrothermal synthesized 3D RGO hydrogel as the sensing element. The 3D RGOH based gas sensor is produced in a simple, high-yield, and cost-effective manner, and it can be deployed to experimentally detect NO_2 and NH_3 with low concentrations of 200 ppb and 20 ppm, respectively. For the first time, locally elevated temperature created by an integrated microheater has been employed to improve the selectivity of NO_2 sensing by quenching the response from NH_3. This strategy provides new insight into improving the selectivity of gas sensing, which may be extended to the improvement of other chemical sensing devices. The microheater is also employed to speed up the signal recovery process. Comparing the sensing performances between 3D RGOH and 2D RGO sensors, we found that the transduction signal of the 3D RGOH devices increased more than 10 times compared to that of 2D RGO devices, demonstrating the usefulness of the 3D porous RGOH nanostructures in gas sensing.

ASSOCIATED CONTENT

Supporting Information

The Supporting Information is available free of charge on the ACS Publications website at DOI: 10.1021/acsami.5b09695.

Characterization of the microheater at different temperatures, response of the RGOH sensor to NO_2 at 55 °C, NO_2 sensing with linearly increased NO_2 concentration, theoretical calculation of noise level, LOD, sensitivity, the saturated response and equilibrium constant, the measured and linearly fitted resistance of the RGOH device versus temperature, response of the RGOH sensor as a function of NH_3 concentration, and the measured Seebeck coefficient of RGOH. (PDF)

AUTHOR INFORMATION

Corresponding Author

*E-mail: MJMMiao@ntu.edu.sg.

Notes

The authors declare no competing financial interest.

ACKNOWLEDGMENTS

This research was funded in part by the Singapore National Research Foundation (NRF) through the Center for Environmental Sensing and Modeling (CENSAM) in Singapore-MIT Alliance for Research and Technology (SMART). We thank all staff and students in the Micromachines Lab 1 for their support in device fabrication.

REFERENCES

(1) Fowler, J. D.; Allen, M. J.; Tung, V. C.; Yang, Y.; Kaner, R. B.; Weiller, B. H. Practical Chemical Sensors from Chemically Derived Graphene. *ACS Nano* **2009**, *3*, 301−306.

(2) Duy, L. T.; Kim, D.-J.; Trung, T. Q.; Dang, V. Q.; Kim, B.-Y.; Moon, H. K.; Lee, N.-E. High Performance Three-Dimensional Chemical Sensor Platform Using Reduced Graphene Oxide Formed on High Aspect-Ratio Micro-Pillars. *Adv. Funct. Mater.* **2015**, *25*, 883−890.

(3) Yuan, W. J.; Liu, A. R.; Huang, L.; Li, C.; Shi, G. Q. High-Performance NO_2 Sensors Based on Chemically Modified Graphene. *Adv. Mater.* **2013**, *25*, 766−771.

(4) Schedin, F.; Geim, A. K.; Morozov, S. V.; Hill, E. W.; Blake, P.; Katsnelson, M. I.; Novoselov, K. S. Detection of Individual Gas Molecules Adsorbed on Graphene. *Nat. Mater.* **2007**, *6*, 652−655.

(5) Yuan, W. J.; Huang, L.; Zhou, Q. Q.; Shi, G. Q. Ultrasensitive and Selective Nitrogen Dioxide Sensor Based on Self-Assembled Graphene/Polymer Composite Nanofibers. *ACS Appl. Mater. Interfaces* **2014**, *6*, 17003−17008.

DOI: 10.1021/acsami.5b09695
ACS Appl. Mater. Interfaces 2015, 7, 27502−27510

(6) Yang, Y. J.; Li, S. B.; Yang, W. Y.; Yuan, W. T.; Xu, J. H.; Jiang, Y. D. In Situ Polymerization Deposition of Porous Conducting Polymer on Reduced Graphene Oxide for Gas Sensor. *ACS Appl. Mater. Interfaces* **2014**, *6*, 13807−13814.
(7) Liu, Y.; Jiao, Y.; Zhang, Z. L.; Qu, F. Y.; Umar, A.; Wu, X. Hierarchical SnO_2 Nanostructures Made of Intermingled Ultrathin Nanosheets for Environmental Remediation, Smart Gas Sensor, and Supercapacitor Applications. *ACS Appl. Mater. Interfaces* **2014**, *6*, 2174−2184.
(8) Ratinac, K. R.; Yang, W.; Ringer, S. P.; Braet, F. Toward Ubiquitous Environmental Gas Sensors-Capitalizing on the Promise of Graphene. *Environ. Sci. Technol.* **2010**, *44*, 1167−1176.
(9) Azzarelli, J. M.; Mirica, K. A.; Ravnsbaek, J. B.; Swager, T. M. Wireless Gas Detection with a Smartphone via Rf Communication. *Proc. Natl. Acad. Sci. U. S. A.* **2014**, *111*, 18162−18166.
(10) Mirica, K. A.; Azzarelli, J. M.; Weis, J. G.; Schnorr, J. M.; Swager, T. M. Rapid Prototyping of Carbon-Based Chemiresistive Gas Sensors on Paper. *Proc. Natl. Acad. Sci. U. S. A.* **2013**, *110*, E3265−E3270.
(11) Franke, M. E.; Koplin, T. J.; Simon, U. Metal and Metal Oxide Nanoparticles in Chemiresistors: Does the Nanoscale Matter? *Small* **2006**, *2*, 36−50.
(12) Liu, Y. X.; Dong, X. C.; Chen, P. Biological and Chemical Sensors Based on Graphene Materials. *Chem. Soc. Rev.* **2012**, *41*, 2283−2307.
(13) Yavari, F.; Chen, Z.; Thomas, A. V.; Ren, W.; Cheng, H. M.; Koratkar, N. High Sensitivity Gas Detection Using a Macroscopic Three-Dimensional Graphene Foam Network. *Sci. Rep.* **2011**, *1*, 166.
(14) Yuan, W. J.; Shi, G. Q. Graphene-Based Gas Sensors. *J. Mater. Chem. A* **2013**, *1*, 10078−10091.
(15) Liu, S.; Yu, B.; Zhang, H.; Fei, T.; Zhang, T. Enhancing NO_2 Gas Sensing Performances at Room Temperature Based on Reduced Graphene Oxide-ZnO Nanoparticles Hybrids. *Sens. Actuators, B* **2014**, *202*, 272−278.
(16) Bai, H.; Sheng, K. X.; Zhang, P. F.; Li, C.; Shi, G. Q. Graphene Oxide/Conducting Polymer Composite Hydrogels. *J. Mater. Chem.* **2011**, *21*, 18653−18658.
(17) Some, S.; Xu, Y.; Kim, Y.; Yoon, Y.; Qin, H. Y.; Kulkarni, A.; Kim, T.; Lee, H. Highly Sensitive and Selective Gas Sensor Using Hydrophilic and Hydrophobic Graphenes. *Sci. Rep.* **2013**, *3*, 1868.
(18) Han, T. H.; Huang, Y. K.; Tan, A. T.; Dravid, V. P.; Huang, J. X. Steam Etched Porous Graphene Oxide Network for Chemical Sensing. *J. Am. Chem. Soc.* **2011**, *133*, 15264−15267.
(19) Robinson, J. T.; Perkins, F. K.; Snow, E. S.; Wei, Z. Q.; Sheehan, P. E. Reduced Graphene Oxide Molecular Sensors. *Nano Lett.* **2008**, *8*, 3137−3140.
(20) Xu, Y. X.; Sheng, K. X.; Li, C.; Shi, G. Q. Self-Assembled Graphene Hydrogel via a One-Step Hydrothermal Process. *ACS Nano* **2010**, *4*, 4324−4330.
(21) Xu, Y. X.; Shi, G. Q.; Duan, X. F. Self-Assembled Three-Dimensional Graphene Macrostructures: Synthesis and Applications in Supercapacitors. *Acc. Chem. Res.* **2015**, *48*, 1666−1675.
(22) Sui, Z. Y.; Cui, Y.; Zhu, J. H.; Han, B. H. Preparation of Three-Dimensional Graphene Oxide-Polyethylenimine Porous Materials as Dye and Gas Adsorbents. *ACS Appl. Mater. Interfaces* **2013**, *5*, 9172−9179.
(23) Yun, Y. J.; Hong, W. G.; Choi, N. J.; Park, H. J.; Moon, S. E.; Kim, B. H.; Song, K. B.; Jun, Y.; Lee, H. K. A 3D Scaffold for Ultra-sensitive Reduced Graphene Oxide Gas Sensors. *Nanoscale* **2014**, *6*, 6511−6514.
(24) Yang, G.; Lee, C.; Kim, J. Three-Dimensional Graphene Network-Based Chemical Sensors on Paper Substrate. *J. Electrochem. Soc.* **2013**, *160*, B160−B163.
(25) Chen, Z.; Ren, W.; Gao, L.; Liu, B.; Pei, S.; Cheng, H. M. Three-Dimensional Flexible and Conductive Interconnected Graphene Networks Grown by Chemical Vapour Deposition. *Nat. Mater.* **2011**, *10*, 424−428.
(26) Jiang, L. L.; Fan, Z. J. Design of Advanced Porous Graphene Materials: from Graphene Nanomesh to 3D Architectures. *Nanoscale* **2014**, *6*, 1922−1945.
(27) Li, L.; He, S. J.; Liu, M. M.; Zhang, C. M.; Chen, W. Three-Dimensional Mesoporous Graphene Aerogel-Supported SnO_2 Nanocrystals for High-Performance NO_2 Gas Sensing at Low Temperature. *Anal. Chem.* **2015**, *87*, 1638−1645.
(28) Wu, J.; Yu, C. H.; Li, S. Z.; Zou, B. H.; Liu, Y. Y.; Zhu, X. Q.; Guo, Y. Y.; Xu, H. B.; Zhang, W. N.; Zhang, L. P.; Liu, B.; Tian, D. B.; Huang, W.; Sheetz, M. P.; Huo, F. W. Parallel Near-Field Photolithography with Metal-Coated Elastomeric Masks. *Langmuir* **2015**, *31*, 1210−1217.
(29) Marcano, D. C.; Kosynkin, D. V.; Berlin, J. M.; Sinitskii, A.; Sun, Z. Z.; Slesarev, A.; Alemany, L. B.; Lu, W.; Tour, J. M. Improved Synthesis of Graphene Oxide. *ACS Nano* **2010**, *4*, 4806−4814.
(30) Lu, J. Y.; Miao, J. M.; Norford, L. K. Localized Synthesis of Horizontally Suspended Carbon Nanotubes. *Carbon* **2013**, *57*, 259−266.
(31) Xu, Y. X.; Lin, Z. Y.; Huang, X. Q.; Wang, Y.; Huang, Y.; Duan, X. F. Functionalized Graphene Hydrogel-Based High-Performance Supercapacitors. *Adv. Mater.* **2013**, *25*, 5779−5784.
(32) Yang, F.; Taggart, D. K.; Penner, R. M. Joule Heating a Palladium Nanowire Sensor for Accelerated Response and Recovery to Hydrogen Gas. *Small* **2010**, *6*, 1422−1429.
(33) Wongwiriyapan, W.; Inoue, S.; Honda, S.-i.; Katayama, M. Adsorption Kinetics of NO_2 on Single-Walled Carbon Nanotube Thin-Film Sensor. *Jpn. J. Appl. Phys.* **2008**, *47*, 8145−8147.
(34) Wongwiriyapan, W.; Honda, S.-i.; Konishi, H.; Mizuta, T.; Ikuno, T.; Ito, T.; Maekawa, T.; Suzuki, K.; Ishikawa, H.; Oura, K.; Katayama, M. Single-Walled Carbon Nanotube Thin-Film Sensor for Ultrasensitive Gas Detection. *Jpn. J. Appl. Phys.* **2005**, *44*, L482−L484.
(35) Hassinen, J.; Kauppila, J.; Leiro, J.; Maattanen, A.; Ihalainen, P.; Peltonen, J.; Lukkari, J. Low-Cost Reduced Graphene Oxide-Based Conductometric Nitrogen Dioxide-Sensitive Sensor on Paper. *Anal. Bioanal. Chem.* **2013**, *405*, 3611−3617.
(36) Dua, V.; Surwade, S. P.; Ammu, S.; Agnihotra, S. R.; Jain, S.; Roberts, K. E.; Park, S.; Ruoff, R. S.; Manohar, S. K. All-Organic Vapor Sensor Using Inkjet-Printed Reduced Graphene Oxide. *Angew. Chem., Int. Ed.* **2010**, *49*, 2154−2157.
(37) Liu, X.; Cui, J. S.; Sun, J. B.; Zhang, X. T. 3D Graphene Aerogel-Supported SnO_2 Nanoparticles for Efficient Detection of NO_2. *RSC Adv.* **2014**, *4*, 22601−22605.
(38) Jayanthi, S.; Mukherjee, A.; Chatterjee, K.; Sood, A. K.; Misra, A. Tailored Nitrogen Dioxide Sensing Response of Three-Dimensional Graphene Foam. *Sens. Actuators, B* **2016**, *222*, 21−27.
(39) Tabata, H.; Fukuda, H.; Matsushita, K.; Kubo, O.; Kikuchi, T.; Sato, T.; Kamimura, T.; Ueda, T.; Shimazaki, R.; Tanjo, H.; Horiuchi, M.; Katayama, M. Metal-Oxide-Layer-Coated Single-Walled Carbon Nanotubes as a Sensor for Trace Amounts of Oxygen. *Appl. Phys. Express* **2014**, *7*, 035101.
(40) Wongwiriyapan, W.; Inoue, S.; Okabayashi, Y.; Ito, T.; Shimazaki, R.; Maekawa, T.; Suzuki, K.; Ishikawa, H.; Honda, S.-i.; Mori, H.; Oura, K.; Katayama, M. Highly Stable and Sensitive Gas Sensor Based on Single-Walled Carbon Nanotubes Protected by Metal-Oxide Coating Layer. *Appl. Phys. Express* **2009**, *2*, 095008.
(41) Chen, R. J.; Franklin, N. R.; Kong, J.; Cao, J.; Tombler, T. W.; Zhang, Y. G.; Dai, H. J. Molecular Photodesorption from Single-Walled Carbon Nanotubes. *Appl. Phys. Lett.* **2001**, *79*, 2258−2260.
(42) Kang, I.-S.; So, H.-M.; Bang, G.-S.; Kwak, J.-H.; Lee, J.-O.; Won Ahn, C. Recovery Improvement of Graphene-Based Gas Sensors Functionalized with Nanoscale Heterojunctions. *Appl. Phys. Lett.* **2012**, *101*, 123504.
(43) ACGIH. In 2005 TLVs and BEIs Based on the Document of the Threshold Limit Values for Chemical Substances and Physical Agents & Biological Exposure Indices. *American Conference of Governmental Industrial Hygienists (ACGIH)*, Cincinnati, Ohio, 2005; pp 8−29.
(44) Li, X. M.; Yin, J.; Zhou, J. X.; Wang, Q.; Guo, W. L. Exceptional High Seebeck Coefficient and Gas-Flow-Induced Voltage in Multilayer Graphene. *Appl. Phys. Lett.* **2012**, *100*, 183108.
(45) Yang, J. Y.; Wu, J.; Li, G.; Zhang, J. S.; Peng, J. Y. Preparation and Thermoelectric Properties of Polycrystalline In_4Sn_{3-x} by

DOI: 10.1021/acsami.5b09695
ACS Appl. Mater. Interfaces 2015, 7, 27502−27510

Mechanical Alloying and Hot Pressing. *J. Electron. Mater.* **2012**, *41*, 1077−1080.
(46) Miller, N.; Ager, J. W.; Smith, H. M.; Mayer, M. A.; Yu, K. M.; Haller, E. E.; Walukiewicz, W.; Schaff, W. J.; Gallinat, C.; Koblmüller, G.; Speck, J. S. Hole Transport and Photoluminescence in Mg-Doped InN. *J. Appl. Phys.* **2010**, *107*, 113712.
(47) Hao, L.; Lee, T. K. Thermopower of Gapped Bilayer Graphene. *Phys. Rev. B: Condens. Matter Mater. Phys.* **2010**, *81*, 165445.
(48) Zhang, Y. H.; Chen, Y. B.; Zhou, K. G.; Liu, C. H.; Zeng, J.; Zhang, H. L.; Peng, Y. Improving Gas Sensing Properties of Graphene by Introducing Dopants and Defects: A First-Principles Study. *Nanotechnology* **2009**, *20*, 185504.
(49) Ben Aziza, Z.; Zhang, Q.; Baillargeat, D. Graphene/Mica Based Ammonia Gas Sensors. *Appl. Phys. Lett.* **2014**, *105*, 254102.
(50) Jeong, H. Y.; Lee, D.-S.; Choi, H. K.; Lee, D. H.; Kim, J.-E.; Lee, J. Y.; Lee, W. J.; Kim, S. O.; Choi, S.-Y. Flexible Room-Temperature NO_2 Gas Sensors Based on Carbon Nanotubes/Reduced Graphene Hybrid Films. *Appl. Phys. Lett.* **2010**, *96*, 213105.
(51) Choi, H.; Choi, J. S.; Kim, J. S.; Choe, J. H.; Chung, K. H.; Shin, J. W.; Kim, J. T.; Youn, D. H.; Kim, K. C.; Lee, J. I.; Choi, S. Y.; Kim, P.; Choi, C. G.; Yu, Y. J. Flexible and Transparent Gas Molecule Sensor Integrated with Sensing and Heating Graphene Layers. *Small* **2014**, *10*, 3685−3691.
(52) He, Q. Y.; Wu, S. X.; Yin, Z. Y.; Zhang, H. Graphene-Based Electronic Sensors. *Chem. Sci.* **2012**, *3*, 1764−1772.
(53) Lipatov, A.; Varezhnikov, A.; Wilson, P.; Sysoev, V.; Kolmakov, A.; Sinitskii, A. Highly Selective Gas Sensor Arrays Based on Thermally Reduced Graphene Oxide. *Nanoscale* **2013**, *5*, 5426−5434.
(54) Lipatov, A.; Varezhnikov, A.; Augustin, M.; Bruns, M.; Sommer, M.; Sysoev, V.; Kolmakov, A.; Sinitskii, A. Intrinsic Device-to-Device Variation in Graphene Field-Effect Transistors on a Si/SiO_2 Substrate as a Platform for Discriminative Gas Sensing. *Appl. Phys. Lett.* **2014**, *104*, 013114.

DOI: 10.1021/acsami.5b09695
ACS Appl. Mater. Interfaces 2015, 7, 27502−27510